Improving optic disk location in fundus camera images by plausible detection

Emanuele Trucco and Hind Azegrouz*

Heriot Watt University, Edinburgh, UK

Abstract. We present a robust constraint satisfaction algorithm to detect the optic disk in retinal images, substantially improving our previous results [1], and matching the performance of, or outperforming, recently reported algorithms. The algorithm locates a number of candidates of optic disk and macula, and the approximate path of the main blood vessels (arcades). The number is high enough that the confidence to include the right landmark is high. The optic disk is detected as member of the triplet disk/macula/arcade which best satisfies a-priori anatomical constraints. The MATLAB prototype was tested on the 63 images of the STARE set [2] including both disk and macula, with only 3 failures (95%).

1 Introduction and related work

We present a robust algorithm to detect the optic disk (OD) in retinal images, based on plausible detection and constraint satisfaction. The algorithm is a substantial improvement on the previous version reported in [1] pushing successful detection from 86% to 95% on the popular STARE test set of fundus camera images [2].

Many retinal image analysis algorithms have been proposed to detect OD, macula and vasculature and to identify disease symptoms [3–11]. Hoover and Goldbaum [6] and Li and Chutatape [12] give recent, concise reviews focussing on OD.

Most approaches aim to generate single, optimal candidates with the highest confidence possible. Here, we are particularly interested in algorithms taking advantage of a-priori knowledge on retinal imagery. Such knowledge derives from *retinal properties*, e.g., the expected shape, position and orientation, relative or absolute, of retinal elements, and from *image formation properties*, i.e., the expected appearance (grey levels and their properties) of retinal elements due to the interaction of the retina with light and sensor. Assumptions about the latter are usually approximate as quantitative models of retinal image formation; they are however complex and not easily incorporated in image processing algorithms. Instead, various retinal properties have been used to counter the variability of retinal appearance due to lesions, diseases, imaging conditions, race, and other factors, which limit the performance of algorithms based purely on relative brightness variations [4, 13]. Hoover and Goldbaum detected the OD as the (fuzzy) convergence region of retinal vessels [6]; Foracchia's *et al.* [14] devised a parametric model of vessel geometry. Extended symbolic schemes have also been reported: e.g., expert systems [15], retina mapping [9] and constraint satisfaction with plausible detection [1].

We deploy simple detectors of OD, macula and arcades to generate sets of *plausible* candidates for each landmark; such sets include the true landmarks with high probability. We then search the space of all possible triplets (OD, macula, arcade) formed by the candidates to identify the one best satisfying constraints imposed by retinal anatomy. The approximate arcades path is found by a simulated annealing search. This statistical algorithm offers excellent optimization performance and can locate plausible paths in the presence of severely altered retinas.

This approach has several advantages. Searching a potentially large space of plausible solutions supports robustness, as it is easier to generate a set of candidates for a given landmark including the true one with high confidence, than to find *only* the true one with the same confidence. Although here success is defined as correct detection of only the OD, the selected triplet contains correct macula and arcades in most cases.

2 The algorithm

2.1 Algorithm outline

The algorithm is organised in two stages. First, independent detectors of OD and maculas as used to generate plausible candidates, and approximate arcades traced. Second, triplets OD/macula/arcades are formed and searched.

*Corresponding author, E-mail: ha19@hw.ac.uk.

OD and macula detection follow our previous work [1], arcade detection and constraint satisfaction are novel. We describe briefly each module below.

2.2 Optic disk detection

This simple detector assumes that the OD is one of the brightest image regions [8], although not necessarily the brightest. First, we apply a 7×7 median filter to attenuate image noise. We then apply morphological closing followed by opening to suppress most of the vasculature information. The structural element is a disk larger than the largest vessel cross-section (8-pixel diameter in our case). Finally, we collect the N_o brightest regions in the image (based on mean region intensity) as plausible OD candidates. These may include diseased areas and possible bright, noisy spots.

2.3 Macula detection

Similarly to the OD detector, we assume that the macula corresponds to one of the darkest image regions. However, unlike the OD, grey levels in the macula region cannot be expected to be significantly darker than the rest of the image, e.g., than major vessels. We use the same, simple detector adopted for the OD, but collect the N_m *darkest* candidates. These may include noisy areas (e.g., peripheral low-intensity spots), diseased areas, nevus, and so forth.

2.4 Arcade detection

We aim to trace the *approximate* path of the arcades, as this is sufficient to constrain the position of macula and OD. This proved a critical step as incorrect detection would cause overall failure. We assume a simple geometric model formed by two horizontal half-parabolas, $x = a_j y^2 + b_j y + c_j$ with $j = 1$ or 2, fitted independently but with vertices constrained to be within an optic disk diameter of each other. Parabola fitting is cast as two optimization problems, each for a half-parabola, in the 3-dimensional parameter space, $\mathbf{v} = [a_j b_j c_j]$. We describe briefly the target function and the optimization algorithm used.

Target function. We aim to optimize a cost coefficient based on the expected intensity profile along a candidate parabola arc. If the latter follows the arcade well, the intensity profile across the arc should correlate well with cross-sections of large vessels, which we take to be Gaussian as commonly done. The image is preliminarily smoothed by a Gaussian filter with $\sigma = 1.5$ to reduce the side peaks due to brighter vessel contours. We use sum of squared difference instead of correlation, yielding a cost function to minimize.

Given a half-parabola candidate $\mathbf{v}_k$, the target function is

$$c(\mathbf{v}_k) = \sum_{i=1}^{N_s} \sum_{h=1}^{N_p} [I_r(h) - I(\mathbf{p}_i^s(h))]^2 \tag{1}$$

where N_s and N_p are the number of, respectively, the segments normal to the arc (20 in our experiments) and the point on each segment (i.e., on each intensity profile). $I_r(h)$ is the h-th intensity on the reference profile, and $I(\mathbf{p}_i^s(h))$ is the image intensity at the the corresponding point on the i-th segment perpendicular to the parabola.

Optimization. Simulated annealing (SA) can explore wide regions of an energy landscape at reasonable computational cost. We refer the reader to [16] for SA details; in essence, SA explores increasingly smaller regions of the search space, the size of which is controlled by a decreasing "temperature" parameter. Points to evaluate are picked at random, and states with worse (higher) energy are accepted again randomly, with probability decreasing with temperature as the algorithm homes in to a solution. This feature allows the algorithm to escape from local minima. In our system, temperature is reduced exponentially as $T = T(0.9)^k$, k the iteration index. The end temperature is chosen so that the probability of accepting lower-energy states is 0.1. We have successfully applied SA search to iris detection in [17].

The parabola concavity is initialized to the average of observed values, and the vertex to the center of the currently explored OD candidate. Our choices of values for SA parameters rely on extensive experimentation carried out in a twin project: tests were run with hundreds of manually ground-truthed images and statistics of location errors plotted. From this, we estimated a-posteriori optimal values for all parameters.

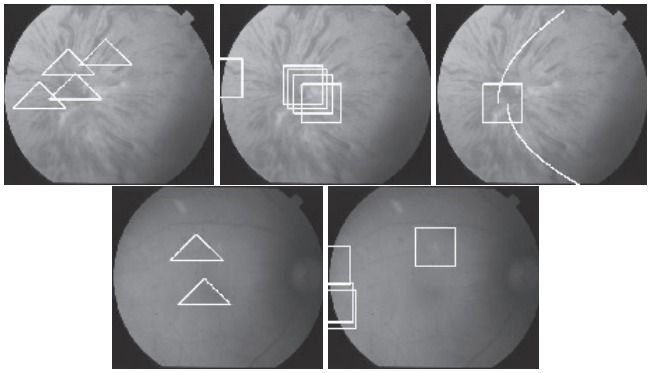

Figure 1. Failure examples. Img026 (top): candidates of macula (left), OD (center), final detection (right). Img013 (bottom): candidates of macula (left) and OD.

2.5 Constraint satisfaction

We must now search the space of the triplets (OD, macula, arcade) generated by combining all plausible candidates to locate the one most consistent with the following anatomical constraints.

1. *The macula must be near the approximate axis of symmetry of the arcade.*
2. *The distance between OD and macula must fall within a pre-defined interval.*
3. *The average contrast along the hypothesized parabola must be high.*

The arcades are forced to converge in the OD by initializing the vertex of the parabola fit to be at the hypothesized OD location. All quantities in the constraints are modelled as Gaussian random variables with mean and standard deviation derived from healthy retina images. Values observed at run time yield probabilities, one per constraint, which are composed assuming independent constraints. The result provides a merit score for each triplet, which is used in the following stage.

Search for the optimal triplet. Even 6 to 10 candidates per OD and macula generate rather relatively small triplet numbers, which can be simply sorted by score in reasonable time. The OD is located as the member of the highest-scoring triplet. More complex schemes like the constraint satisfaction one reported in [1]do not introduce advantages for small search spaces, but become necessary if further elements are considered (e.g., disease symptoms) causing the search space to grow rapidly.

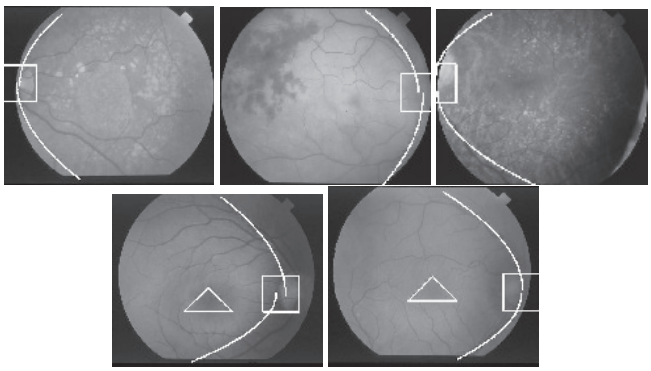

Figure 2. Top: examples of correct OD detection (3, 20, 41); notice that 41 is a difficult case for [14]. Bottom: Examples of full triplet detection (imgs 240, 219), normally achieved when the OD is located correctly.

3 Experimental results

An initial prototype has been implemented in MATLAB on a 2.4GHz PC under XP. The diameter of the disk used as structural element in the morphology-based OD and macula detection was 8 pixels throughout. We consider the

OD successfully located if its center falls within 60 pixels (average OD radius in STARE images) of the manually located center of the true OD region. This is in essence the same criterion used in [6], which facilitates comparison.

We tested our system on the STARE test set of 605×700 images [2] acquired by a Topcon TRV-50 fundus camera with 35° field of view. Given our assumptions, we considered only the 63 images capturing a region including both macula and OD, even if not necessarily visible. This subset included several retinas showing severe disease symptoms. We allowed a maximum of 10 candidates per detector for OD and macula ($N_o = N_m = 10$). Detection was successful in 60 out of 63 images (95.24% success), outperforming [6] (86% success over the whole set). Common failures were img 13 and 26 (the latter a very corrupted retina), shown in Figure 1. Our system could correctly detect the OD in images 7, 19, 27, 139, on which [6] failed or did not conclude. Figure 2 shows examples of successful detection with diseased images. Performance is very close to Foracchia's *et al* algorithm [14], who report only 4 failures on the full 81-image set; our algorithm, module by module, is arguably simpler. Performance is similar or better than that of several other algorithms reported recently, but comparisons based on reports is made difficult by the use of independent data sets [12, 18, 19].

4 Conclusions

We have presented a robust algorithm to detect the optic disk in retinal images, substantially improving the detection rate of our previous work [1] and matching the performance of, or outperforming, recently reported algorithms. Current results show the excellent potential of the approach to incorporate disease symptoms, towards an integrated retina mapping and computer-assisted diagnosis system for fundus camera images. Further future work is planned on an experimental, comparative evaluation of recent OD algorithms on an extensive test set, including normal and wide field of views.

References

1. E. Trucco & P. J. Kamat. "Locating the optic disk in images via plausible detection and constraint satisfaction." In *Proc. IEEE Int.Conf. on Image Processing*. 2004.
2. STARE data. "www.parl.clemson.edu/stare/nerve/."
3. A. Can, H. Shen, J. N. Turner et al. "Rapid automatic tracing and feature extraction from retinal fundus images using direct exploratory algorithms." *IEEE Trans. Information Technology in Biomedicine* **3(3)**, pp. 125–138, 1999.
4. S. Chauduri, S. Chatterjee, N. Katz et al. "Automatic detection of the optic nerve in retinal images." In *Proc. IEEE Int.Conf. on Image Processing*, pp. 1–5. 1989.
5. A. Can, C. Stewart, B. Roysam et al. "A feature-based robust hierachical algorithm for registering pairs of images of the human retina." *IEEE Trans. Pattern Analysis and Machine Intelligence* **24(3)**, 2002.
6. A. Hoover & M. Goldbaum. "Locating the optic nerve in a retinal image using the fuzzy convergence of the blood vessels." *IEEE Trans. Medical Imaging* **22(8)**, pp. 951–8, 2003.
7. X. Jiang & D. Mojon. "Adaptive local thresholding by verification-based multithreshold probing with an application to vessel detection in retinal images." *IEEE Trans. Pattern Analysis and Machine Intelligence* **25(1)**, pp. 131–7, 2003.
8. H. Li & O. Chutatape. "Automatic location of the optic disk in retinal images." In *Proc. IEEE Int.Conf. on Image Processing*, volume 2, pp. 837–840. 2001.
9. A. Pinz, S. Bernogger, P. Datlinger et al. "Mapping the human retina." *IEEE Trans. Medical Imaging* **17(4)**, pp. 606–619, 1998.
10. F. Zana & J.-C. Klein. "Segmentation of vessel-like patterns using mathematical morphology and curvature evaluation." *IEEE Trans. Image Processing* **10(7)**, pp. 1010–1019, 1998.
11. A. Osareh, M. Mirmehdi, B. Thomas et al. "Identification of exudate pathologies and the optic disc in colour retinal images." *British Journal of Ophthalmology* **87**, pp. 1220–1223.
12. H. Li & O. Chutatape. "Automated feature extraction in color retinal images by a model based approach." In *IEEE Trans. Biomedical Engineering*, volume 51, pp. 246 – 254. 2004.
13. C. Sinthanayothin, J. F. Boyce, H. L. Cook et al. "Automated localization of the optic disc, fovea, and retinal blood vessels from digital color fundus images." *British Journal of Ophtalmology* **83**, pp. 902–910.
14. M. Foracchia, E. Grisan & A. Ruggeri. "Detection of optic disc in retinal images by means of a geometrical model of vessel structure." *IEEE Trans. Medical Imaging* **23(10)**, pp. 1189 – 1195, 2004.
15. M. Gauldbaum, S. Moezzi, A. Taylor et al. "Automatic diagnosis and image understanding with object extraction, classification, and inferencing in retinal images." In *Proc. IEEE Int.Conf. on Image Processing*. 1996.
16. R. Fletcher. *Practical methods of optimization*. Wiley, 1987 (second edition).
17. M. Razeto & E. Trucco. "Robust iris location in close-up images of the eye." In *Pattern Analysis and Applications*. 2005.
18. A. Osareh, M. Mirmehdi, B. Thomas et al. "Comparison of colour spaces for optic disc localisation in retinal images." In *Proc. Int.Conf. on Pattern Recognition*, volume 1, pp. 743 – 746. 2002.
19. M. Lalonde, M. Beaulieu & L. Gagnon. "Fast and robust optic disc detection using pyramidal decomposition and hausdorff-based template matching." *IEEE Trans. Medical Imaging* **20(11)**, pp. 1193 – 1200, 2001.